Shallow electron states of bounded intrinsic stacking faults in silicon

Niklas Lehto
Department of Physics, Luleå University of Technology, S-971 87 Luleå, Sweden
(Received 30 September 1996; revised manuscript received 23 January 1997)

The electronic structure of bounded intrinsic stacking faults in silicon is studied. Especially the influence of the stacking fault width on the electronic states in the band gap is investigated. The extended defect studied comprises an intrinsic stacking fault with two reconstructed 90° partials as boundaries. The atomic structure is determined by different valence force fields. These are the Keating potential, the bond-charge model, and an anharmonic version of the bond-charge model. The electronic structure is calculated by linear combinations of atomic orbitals. Ten Gaussian-type atomic orbitals of s-, p-, and d-type are used, and up to fourth-nearest-neighbor interactions are taken into account. The levels in the band gap are evaluated by the recursion method for nonorthogonal basis functions, and by a continued fraction representation of the local density of states. [S0163-1829(97)00323-8]

I. INTRODUCTION

Electronic and structural properties of extended defects in silicon have attracted considerable attention see, e.g., the reviews by Labusch and Shröter,[1] Alexander,[2] or Alexander and Teichler.[3] This is not surprising, since it is known that such defects in the active region of silicon devices degrade the performance of these devices. This problem is seen in both integrated circuits and high voltage devices. Most studies concentrate on bond-breaking defects, such as dislocations and vacancies. In contrast, there are few investigations of stacking faults. This is due to experimental and calculational difficulties resulting from the small energies involved.

Since stacking faults are produced when perfect dislocations split into partial dislocations, stacking faults and dislocations are unambiguously linked. Therefore it is important to study stacking faults if an understanding of the electronic properties of extended defects is wanted. Such knowledge may be of help in the design of new devices.

An important question is if there exist, within the gap, electronic energy levels that are associated with a defect. Since most interest has been focused on the dislocation core states, there are few experimental investigations of stacking faults. However, Weber and Alexander,[4] using photoluminescence spectra of plastically deformed silicon, observed a stacking fault state at approximately $E_v+0.15$ eV.

This work is a theoretical investigation of the electronic energy levels associated with bounded intrinsic stacking faults. It is focused on how the energy levels within the gap are influenced by the width of the stacking fault. The outline of the paper is as follows. In the next section the geometry of the bounded stacking fault is described. The unit cells are presented in Sec. III. Section IV describes the calculational method used to determine the electronic structure of the stacking faults. The results are presented in Sec. V and discussed in the concluding Sec. VI.

II. GEOMETRY OF THE BOUNDED STACKING FAULT

Silicon crystallizes in the diamond structure, which corresponds to two interpenetrating fcc lattices, one of which is displaced by $(\frac{1}{4},\frac{1}{4},\frac{1}{4})$ with respect to the other. The atoms in the two lattices do not have identical surroundings, so the structure can be described by an fcc lattice with a basis of two atoms per unit cell. Therefore, dislocations in the diamond structure are expected to be similar to dislocations in fcc metals.

In fcc metals the main slip planes are the $\{111\}$ planes, and the major slip directions are $\langle 110\rangle$. The smallest perfect Burgers vector is $\frac{1}{2}\langle 110\rangle$. There are two perfect dislocations with Burgers vectors and dislocation lines along $\langle 110\rangle$ directions. One is a pure screw and the other is a 60° dislocation. These perfect dislocations can dissociate into two partial ones. The 60° dislocation splits into one 30° and one 90° partial, while for the screw dislocation two 30° partials are formed. These partials are separated by a low-energy stacking fault, which is a planar defect corresponding to errors in the stacking sequence in the $\langle 111\rangle$ direction. This fault is due to relative displacements of $\{111\}$ planes by $\frac{1}{6}\langle 211\rangle$. This type of dissociation into two partials reduces the strain energy associated with the dislocation. The size of the stacking fault is determined by the balance of the $1/r$ repulsion between the partials, with the constant attractive force resulting from the formation of the stacking fault.

The same characteristics are found in the diamond lattice. However, the existence of two sublattices generates a layer structure containing $\{111\}$ planes in the sequence $\ldots AaBbCcAaBb\ldots$, where the pairs of planes with the same indices, e.g., Aa, project the same positions on $\{111\}$. The distance between the subsequent planes in one pair, e.g., A and a, is three times longer than the distance between two subsequent planes in different pairs, e.g., a and B. Therefore, there are two distinct types of $\{111\}$ glide planes in the diamond lattice, the one between planes in one pair, which is called the ''shuffle plane'' and the one between different pairs, which is called the ''glide plane.'' The existence of two distinct types of glide planes results in two sets of dislocations with quite different core structures.

Only the ''glide-set'' dislocations have properties similar to dislocations in fcc metals, so dislocations in this set can dissociate into partials separated by a low-energy stacking fault. The dissociation into partials was experimentally ob-

0163-1829/97/55(23)/15601(7)/$10.00 © 1997 The American Physical Society

served in silicon and germanium by the weak-beam technique of electron microscopy.[5–7]

The stacking fault separating the partial dislocations is found to be either intrinsic or extrinsic, but in silicon a majority is of intrinsic character.[8] These low-energy stacking faults involve the insertion or removal of pairs of planes with the same indices; Aa, Bb, etc. The layer structure of an intrinsic fault is $\dots AaBbCc\dagger BbCcAa\dots$, where † indicates an absent Aa plane. In silicon the width of the stacking fault separating the two partials in a dissociated dislocation is about 40 Å for the screw dislocation and 65 Å for the 60° dislocation.[8]

III. GEOMETRY OF THE UNIT CELLS

A theoretical study of extended defects is restricted to a finite and relatively small number of atoms. There are two approximation methods which could be used in the study. The first is to construct a large finite cluster surrounding the defect. However, it is likely then that the influence from the surface of the cluster would mask the more subtle electronic effects of the stacking fault studied here. The second method, which is used in this work, is the large unit cell method. This method involves forming an infinite superlattice of defects by periodically repeating a large unit cell. The use of periodic boundary conditions requires that the sum of the Burgers vectors in the unit cell is zero, since otherwise the elastic strain energy of the crystal would be infinite. This means that the cell must contain at least two dislocations and if it contains two the Burgers vectors must be equal in magnitude and opposite in direction for the two dislocations.

In the most realistic study of the electronic effects from the stacking fault the unit cell should contain a pair of dissociated perfect dislocations with opposite Burgers vectors, which means four partials. This would lead to a very large unit cell. To restrain the size of the problem one of the partials in a dissociated perfect dislocation could be replaced by a different partial so that the sum of the Burgers vectors of the two partials is zero. This means that the unit cell only needs to contain two 30° partials or two 90° partials.

The strain field is influenced by this exchange. However, this deficiency does not alter the topology of the stacking fault.

In silicon the partials are reconstructed. This means that the unit cell length along the dislocation lines must correspond to the periodicity of the reconstruction of the partials. For the reconstructed 30° partials this length is twice as long as for the reconstructed 90° partials, i.e., the 30° partials requires twice as many atoms.

A unit cell withholding one intrinsic stacking fault with two reconstructed 90° partials as boundaries implies that the number of atoms in the cell is reduced by roughly a factor of four compared with the most realistic case. Therefore this type of cell is used in this work.

There is one additional consideration that must be taken into account when the unit cells are constructed. Generally unit cells containing dislocations will generate grain boundaries when the cell is repeated periodically. Unless the size of the cell is commensurate with the periodicity of the grain boundaries a misfit is introduced at the cell boundaries. One way to avoid this is to construct a unit cell so that a quadrupolar lattice of dislocations is generated. This avoids the generation of grain boundaries altogether, which means that the unit cells can be joined without any misfit at the cell boundaries.

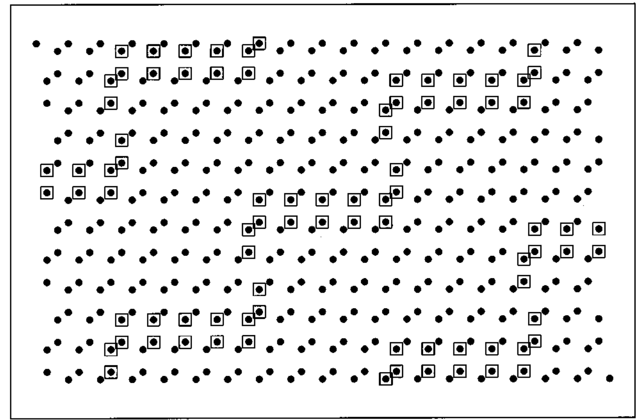

FIG. 1. A projection of an ideal diamond lattice on the (110) plane. Cuts are made in zig-zag patterns and the atoms indicated by squares are removed from the crystal. The horizontal parts of the cuts will generate the intrinsic stacking faults and the vertical cuts will generate the 90° partials. From the resulting crystal the 64-atom unit cell shown in Fig. 2 is obtained.

In this work the construction of the unit cells starts from an ideal crystal. Cuts are made in zig-zag patterns through this crystal as shown in Fig. 1, where the atoms indicated by squares are removed. The horizontal cuts will generate the intrinsic stacking fault and the vertical cuts will generate the 90° partials. Next linear elasticity theory is used to find a first approximation to the atomic structure. Finally an oblique unit cell, containing two dislocations and one intrinsic stacking fault, is constructed. A resulting 64-atom unit cell is seen in Fig. 2. The primitive translation vectors of this super lattice are obtained from the primitive translation vectors of the ideal crystal and the Burgers vectors of the partials. This means that the average density is assumed to be unchanged when the defects are introduced in the crystal.

The final atomic structure of the unit cells is obtained by using different valence force fields. The ones used are the Keating potential,[9] the bond-charge model,[10] and an anharmonic version of the bond-charge model.[11] The Keating potential accurately reproduces the elastic constants or simu-

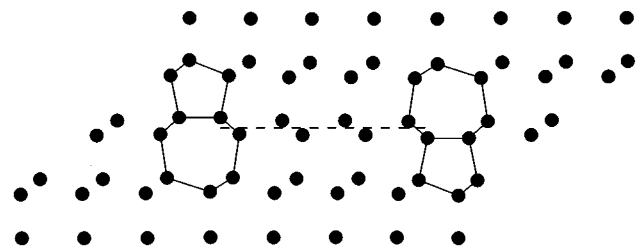

FIG. 2. The 64-atom unit cell projected on the xy plane. The cell contains one stacking fault, which is about 13 Å wide (dashed line), bounded by two reconstructed 90° partials (solid lines) with opposite Burgers vectors.

lates the phonon softening depending on the choice of parameters. The bond-charge model simultaneously reproduces the elastic constants and the phonon softening. The anharmonic version of the bond-charge model reproduces, in addition, the third order elastic constants and gives a more realistic form on the potential between two atoms than the other two valence force fields.

IV. ELECTRONIC STRUCTURE CALCULATIONS

The electronic structure of the stacking faults is calculated using linear combinations of atomic orbitals, which is a very convenient choice of basis functions for band-structure calculations.[12,13] The Schrödinger equation, which determines the band structure $E_n(\boldsymbol{k})$, is

$$\left[-\frac{\hbar^2}{2m}\nabla^2+V(\boldsymbol{r})\right]\psi_n(\boldsymbol{k},\boldsymbol{r})=E_n(\boldsymbol{k})\psi_n(\boldsymbol{k},\boldsymbol{r}), \tag{1}$$

where $\psi_n(\boldsymbol{k},\boldsymbol{r})$ refers to a Bloch function with wave vector $\boldsymbol{k}$.

The potential $V(\boldsymbol{r})$ is a sum of atomic potentials $v(\boldsymbol{r})$, $V(\boldsymbol{r})=\Sigma v(\boldsymbol{r})$, where $v(\boldsymbol{r}+\boldsymbol{R}_\mu)=v(\boldsymbol{r})$ for any atomic site $\boldsymbol{R}_\mu$ in the crystal. The atomic potential is represented by spherical Gaussians as

$$v(r)=\beta_1 e^{-\alpha_1 r^2}+\beta_2 e^{-\alpha_2 r^2}, \tag{2}$$

where $\beta_1=20.0$, $\beta_2=-17.7$, $\alpha_1=0.633$, and $\alpha_2=0.459$ in atomic units.[14]

A set of functions, u_i, localized on the atoms of the crystal is used to expand the Bloch functions ψ_n. The function $u_i(\boldsymbol{r}-\boldsymbol{R}_\mu)$ denotes the ith function on the atomic site $\boldsymbol{R}_\mu$. The functions used are Gaussian orbitals of the form

$$u_i(\boldsymbol{r})=N_i r^l e^{-\xi r^2}K_{l,j}(\hat{r}), \tag{3}$$

in which N_i is a normalization constant, ξ is a decay constant, and $K_{l,j}(\hat{r})$ is a Kubic harmonic. In this study two s-like, three p-like, and five d-like Gaussian orbitals are used. The two s orbitals have, respectively, $\xi=0.19$ and $\xi=0.31$, and the other orbitals have $\xi=0.19$.

The advantage of employing Gaussians to describe the potential and basis orbitals is that all matrix elements in the Hamiltonian and overlap matrices can be expressed analytically. Interactions up to fourth-nearest neighbors are included in the calculations, since this accurately reproduces the band structure of silicon based on plane waves when the above orbitals and potential are used.[14]

The basis functions are nonorthogonal. This means that the problem of determining the electronic structure of the crystal is turned into the problem of solving a generalized eigenvalue problem. Since the unit cells in the study of the bounded stacking fault contain up to about 2000 atoms, and each atom is described by ten basis functions, the dimension of the eigenvalue problem is roughly 20 000. Therefore usual solving methods may not be used. Instead the electronic structure is evaluated by the recursion method for nonorthogonal basis functions.[14,15] In this method the quantum mechanical problem is transformed into a chain model starting on a state $|u_0\rangle$, called the seed state. This means that the generalized eigenvalue problem is now represented by a tridiagonal Jacobi matrix. The energy of the states in the band gap are determined by calculating the eigenvalues of this tridiagonal Jacobi matrix and the orbitals which give these states are determined by evaluating the local density of states in the way described by, e.g., Wang and Lindefelt.[14]

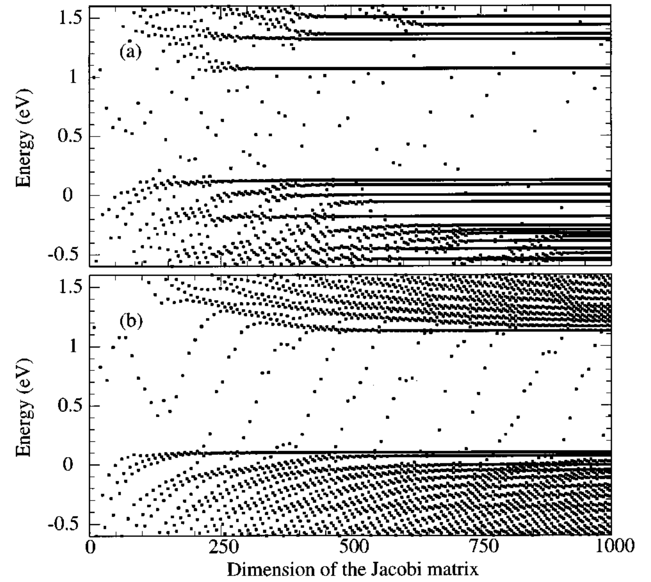

FIG. 3. Eigenvalues of the Jacobi matrix vs matrix dimension. The valence band maximum (E_v) of the ideal structure is at *zero* eV. The seed state is a simple linear combination of p orbitals on four different atoms in the center of the stacking fault. In (a) the unit cell is a 196-atom cell relaxed with the anharmonic bond-charge method and in (b) the unit cell is a 1936-atom cell relaxed with the same valence force field. The shallow states near (E_v) are well converged after about 500 recursion steps even for the larger cell.

In Fig. 3 the convergence of the eigenvalues of the Jacobi matrix is shown for one 196-atom and one 1936-atom unit cell. The states near the valence band maximum are well converged after about 500 recursion steps even for the larger cell. To get a correct prediction of the energies of the electronic states, 1000 recursion steps are used in this study of the bounded intrinsic stacking fault.

V. RESULTS

The infinite intrinsic stacking fault is used as a reference system in this work. Earlier investigations of infinite intrinsic stacking faults in silicon,[16–19] show that these faults generate doubly degenerated shallow electronic states at the Brillouin zone center. These states are occupied and have an energy about 0.1 eV above the valence band maximum (E_v) and they split and bend rapidly into the valence band when leaving the Brillouin zone center.

Here, as in the earlier works,[16–19] the electronic structure of the infinite intrinsic stacking fault is calculated using a small hexagonal unit cell. This unit cell generates a crystal with faults extending infinitely in the basal plane and repeat-

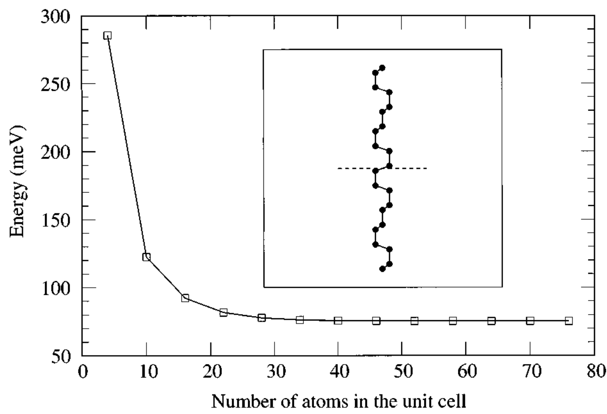

FIG. 4. The energy of the doubly degenerate fault state of an infinite intrinsic stacking fault as a function of the number of atoms in the unit cell. The number of atoms is proportional to the distance between two adjacent fault planes. The valence band maximum (E_v) of the ideal structure is at *zero* eV. The inset shows the type of unit cell used in the calculation. The stacking fault plane is indicated by the dashed line.

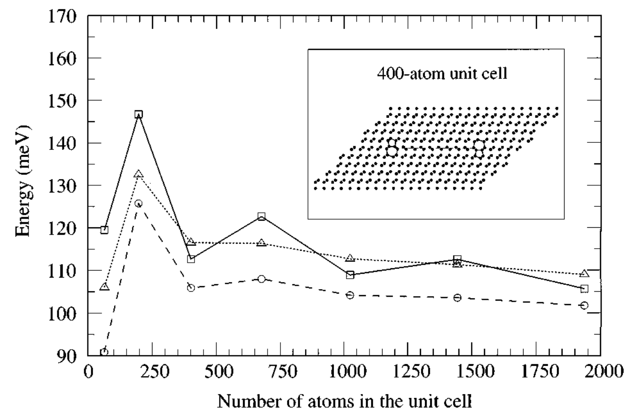

FIG. 5. The energy of the fault state of an intrinsic stacking fault bounded by two 90° partials as a function of the number of atoms in the unit cell. The square root of the number of atoms is proportional to the width of the stacking fault. The atomic structure is determined by the Keating model (squares and solid line), the bond-charge model (triangles and dotted line), and the anharmonic bond-charge model (circles and dashed line). The valence band maximum (E_v) of the ideal structure is at *zero* eV. The inset shows a 400-atom unit cell used in the calculation.

ing periodically normal to it. Ideal bounding lengths and angles are used, since this is what is predicted for this system by the valence force fields used in the atomic structure relaxation of the bounded stacking faults. The distance between two adjacent fault planes is determined by the number of atoms in the hexagonal unit cell. The number of atoms in the cells is varied from 4 to 76 atoms, which means that the distance between adjacent fault planes varies from 6.3 Å to 119 Å.

In Fig. 4 the energy of the doubly degenerate fault state is seen as a function of the number of atoms in the unit cell, which, in turn, is proportional to the distance between adjacent fault planes. The energy of this fault state converges exponentially to E_v+75 meV when the distance is increased. This is somewhat lower than the energy found in the works cited above, but this is due to the larger unit cells used here. The electronic fault states are due to p orbitals in the plane of the stacking fault, whereas the p orbitals perpendicular to the stacking fault do not contribute to the states in the band gap.

In the study of the bounded intrinsic stacking fault seven unit cells of different sizes where used. These cells contain 64, 196, 400, 676, 1024, 1444, and 1936 atoms. The stacking fault width is proportional to the square root of the number of atoms in the unit cell. The width is about 13 Å for the smallest cell and about 70 Å for the 1936-atom cell. Thus the largest cell contains a stacking fault which is wider than the experimentally observed width of 65 Å. These oblique unit cells generate quadrupolar lattices of dislocations as discussed in Sec. IV. Since the fault states due to infinite intrinsic stacking fault are seen in the Brillouin zone center the electronic structure of the bounded faults is calculated for $\boldsymbol{k}=\boldsymbol{0}$, i.e., in the Brillouin zone center.

In Fig. 5 the energy of the fault states is plotted vs the number of atoms in the unit cell. The energy of these states alternates between higher and lower values when the cell size is increased, but it approaches a value slightly above E_v+100 meV for the larger cells. The alternation in energy is due to the fact that the cells with 64, 400, 1024, and 1936 atoms are rotationally symmetric about the center of the cell, while the cell with 196, 676, and 1444 atoms are inversionally symmetric about the cell center. The energy is somewhat lower in the rotationally symmetric cells than in the inversionally symmetric ones, but it must converge to the same value, since the symmetry is insignificant when the width of the stacking fault is large (infinite). It should also converge to the value E_v+75 meV of the infinite stacking fault when the width goes to infinity, but the convergence is seen to be very slow.

These fault states are ascribed to the stacking fault since they are localized in its vicinity. This is seen in Fig. 6, where

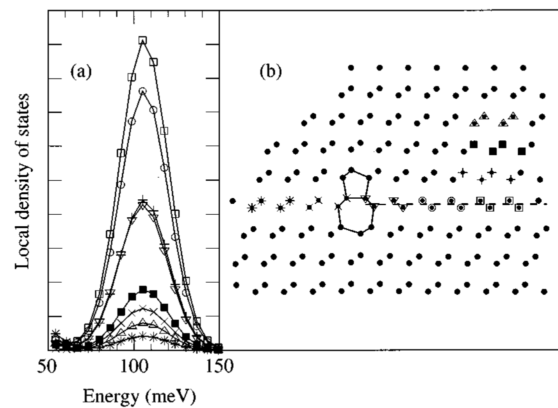

FIG. 6. (a) The local density of states of the fault state in the 400-atom unit cell relaxed by the anharmonic bond-charge model. The density of states is projected on the eight different seed states shown in (b). (b) Each seed state is a linear combination of p orbitals on four atoms. The positions of the four atoms are shown by the symbols. The atoms marked by squares are at the center of the bounded stacking fault.

the local density of states (LDOS) of the fault state in the 400-atom unit cell relaxed by the anharmonic bond charge model is shown. The density of states is projected on different positioned seed states where each seed state is a linear combination of p orbitals on four atoms. The LDOS of the fault state is highest in the center of the stacking fault. It decreases when the seed state is moved away perpendicularly from the stacking fault. The local density of states also decreases when the seed state is moved closer to one of the partials on the stacking fault side and almost vanishes between the partial dislocations on the perfect material side.

The influence of the bounding partial dislocations on the states in the band gap is significant in the smallest unit cells. For the ideal infinite intrinsic stacking fault it is the p orbitals in the stacking fault plane ($p_{\parallel}$) that give rise to the states in the band gap as discussed above. When the same investigation is done on the 64-atom unit cells it is found that it is the p orbitals perpendicular to the fault plane ($p_{\perp}$) that give the most significant contribution to the states in the band gap. These orbitals do not contribute at all to the fault states due to an infinite stacking fault. The contribution from $p_{\perp}$ to the shallow states decreases as the size of the cell is increased. For the largest unit cells it is $p_{\parallel}$ that give rise to the deepest (shallow) states in the band gap, as in the infinite case. That $p_{\perp}$ contributes to the fault states in the smaller cells and that reverse is the case for the larger cells as well as for the ideal infinite fault, depends on the larger deformations introduced in the crystal when the dislocation density is increased.

In the 64-atom unit cells it is the $p_{\perp}$ that give the deepest electronic states. This can be explained if one looks at the spatial extension of their wave functions. The wave functions made up of $p_{\perp}$ penetrate deeper into the perfect material side of the partials than the wave functions composed of $p_{\parallel}$. Therefore, there is a larger overlap between the fault wave functions of $p_{\perp}$ character on neighboring stacking faults than between those of $p_{\parallel}$ character, which in turn accounts for the significant contribution of $p_{\perp}$ to the states in the band gap in the smallest cells. The fact that larger overlap between the fault wave functions cause deeper states is confirmed by a calculation on an ideal intrinsic stacking fault interrupted by rows of vacancies in the fault plane.

In Fig. 5 it is seen that the three models used to determine the atomic structure of the unit cells give rise to a disparity in the prediction of the energy of the states in the band gap. This disparity is largest for the small unit cells and diminishes when the cell is enlarged.

The disparity in the prediction of the energy of the states in the band gap between the three different valence force fields is due to the fact that they produce different atomic structures for the unit cells. The largest difference in the produced atomic structures is found in the cores of the partial dislocations. Figures 7 and 8 show the largest deviations of bond angles and bond lengths compared to ideal bonding vs the size of the unit cell. These most deformed bonds are found in the cores of the reconstructed 90° partial dislocations for all the relaxed structures. The anharmonic bond-charge model produces the largest bond angle deviations, the harmonic bond-charge model gives rise to somewhat smaller bond angle deformations, and the Keating model results in the smallest deviations from ideal bond angles. In Fig. 7 it is seen that the largest deformations of bond angles converge to definite values as the number of atoms in the unit cell is increased. This convergence is most rapid for the anharmonic bond-charge model. The Keating model has a wiggling convergence of the bond angles, which indicates that

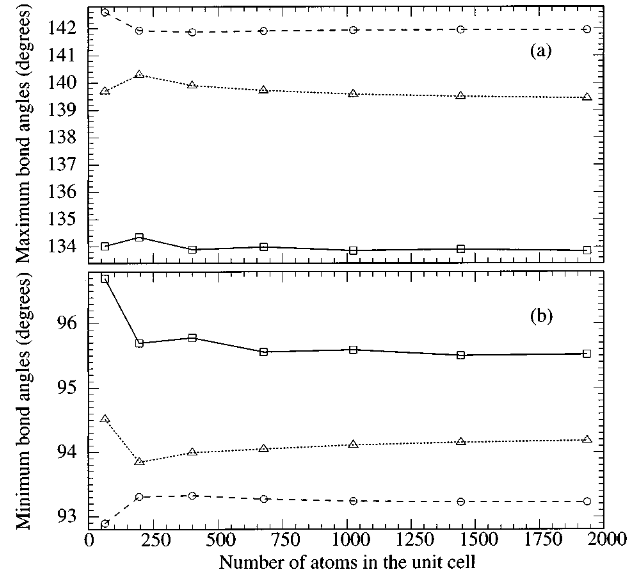

FIG. 7. The maximum (a) and minimum (b) bond angles found in the unit cells as a function of the number of atoms in the cell. The largest deviations from the ideal bond angle (109.47°) are found in the cores of the partial dislocations. The atomic structures are determined by the Keating model (squares and solid line), the bond-charge model (triangles and dotted line), and the anharmonic bond-charge model (circles and dashed line).

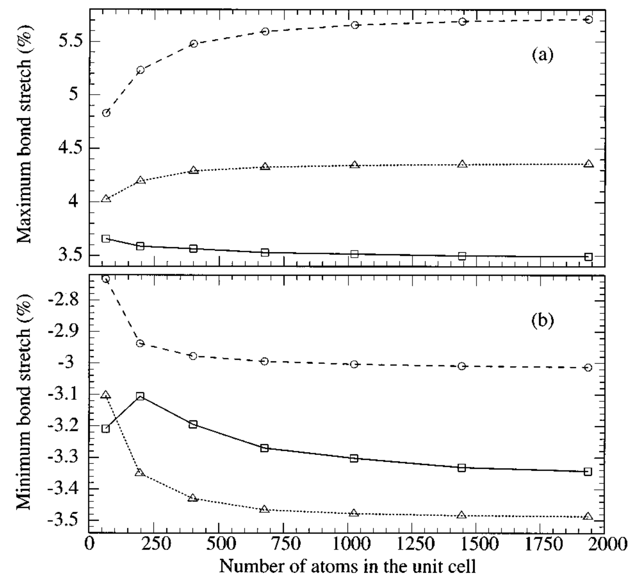

FIG. 8. The maximum (a) and minimum (b) bond expansions found in the unit cells as a function of the number of atoms in the cell. The largest deviations from the ideal bond length (2.35 Å) are found in the cores of the partial dislocations. The atomic structures are determined by the Keating model (squares and solid line), the bond-charge model (triangles and dotted line), and the anharmonic bond-charge model (circles and dashed line).

the core structure obtained with this model is influenced by the symmetry of the unit cell. This is reflected in the calculated energy of the states in the band gap, where the wiggling character is very distinct for the cells relaxed with the Keating model.

Figure 8 shows that the largest deformations of bond lengths also converge to definite values as the number of atoms in the unit cell is increased. The Keating model produces maximum bond stretches of about 3.5% and maximum bond compressions of about 3.3%, so they are of the same magnitude. The bond-charge model gives rise to larger bond length deformations than the Keating model. They are found to be about 4.3% for the maximum and -3.5% for the minimum bond expansions. Thus the maximum bond stretch is somewhat larger than the maximum bond compression when the bond-charge model is used. The anharmonic bond-charge model produces bond length deformations quite different from the other two models. This model causes maximum bond compressions of about 3.0% and maximum bond stretches of about 5.7%, i.e., the maximum bond stretches are almost twice as large as the maximum bond compressions.

VI. SUMMARY AND CONCLUSIONS

In this work shallow electronic states are predicted to exist in silicon when intrinsic stacking faults bounded by partial dislocations are present in the material. Such states are also found in silicon containing infinite intrinsic stacking faults. In this case the states are located at E_v+75 meV when the fault planes are so far apart that there is no interaction between these planes. The states are occupied and are localized near the Brillouin zone center in the reciprocal space and near the stacking fault plane in real space. In the case of a bounded intrinsic stacking fault width of 70 Å, the shallow state is localized between E_v+102 meV and E_v+109 meV, depending on the method used to calculate the atomic structure. From this it is clear that the core structure of the partial dislocations has an almost negligible influence on the stacking fault states. The wave function of the fault states are found to be localized in the vicinity of the stacking fault ribbon. It is also found that the bounding of the stacking fault have a pronounced effect on the shallow states when the partials are close together, i.e., when the overlap of the fault states is not negligible. The effect of this overlap is to lower the energy of the fault states and to change the type of orbitals contributing to the wave function of the deepest state.

The energy of the fault states is predicted to be higher for a bounded stacking fault than for an infinite one, which is an effect of the elastic strain field, present in the first case, due to the partial dislocations. The confinement of the wave functions of these states to the stacking fault ribbon seems to lower the energy, but this effect is small. That the energy of the fault states is higher for a bounded fault is probably valid also for a real dissociated dislocation, even though the elastic strain field is somewhat different in that case. This assumption is confirmed by a calculation on a 504-atom unit cell containing an intrinsic stacking fault bounded by two 30° partials. The width of the stacking fault is about 23 Å, which is slightly wider than for the 196-atom cell containing 90° partials. For this 504-atom cell fault states are found at E_v+210 meV, which is about 60 meV higher than what is found for the 196-atom cell. Consequently this effect should be even more distinct for a real dissociated dislocation than for the stacking fault bounded by 90° partials.

The energy of the shallow stacking fault states calculated in this work is of the same order of magnitude as the experimental value of $E_v+0.15$ eV found by Weber and Alexander.[4] In a study of the electronic structure of reconstructed 90° partials by Lodge *et al.*,[20] stacking fault levels were found at $E_v+0.11$ eV in a 64-atom unit cell containing two partials. Their result is in excellent agreement with the energy calculated here for the 64-atom unit cell relaxed with the bond-charge model. In contrast fault levels at $E_v+0.3$ eV were found using a nonoblique 256-atom unit cell.[18] The notably higher energy found in that work is due to the artificial elastic stress introduced in the lattice by lattice misfit at the cell boundaries. This misfit, in turn, is due to the low angle grain boundary present in the crystal generated by that nonoblique cell (see Sec. III).

At present the only experimental findings, known to the author, that verify the existence of the fault levels reported here is the work by Weber and Alexander.[4] However, the calculations done in this work show that shallow states in the band gap appear when clean stacking fault ribbons are introduced in silicon.

Since stacking fault ribbons in general are not clean, there is a need to investigate how point defects in these extended defects influence the electronic properties of silicon. Thus the electronic properties of extended defects in silicon are not yet entirely known, but this work increases the understanding of how the electronic structure is affected by stacking faults, especially when the faults are due to dissociated perfect dislocations.

[1] R. Labusch and W. Schröter, in *Dislocations in Solids*, edited by F.R.N. Nabarro (North-Holland, Amsterdam, 1980), Vol. 5, p. 128.

[2] H. Alexander, in *Dislocations in Solids* (Ref. 1), Vol. 7, p. 118.

[3] H. Alexander and H. Teichler, in *Materials Science and Technology*, edited by R.W. Cahn, P. Haasen, and E.J. Kramer (VCH Weinheim, Cambridge, 1993), Vol. 4, p. 249.

[4] E.R. Weber and H. Alexander, J. Phys. Paris (Colloq.) **4**, C-319 (1983).

[5] I.L.F. Ray and D.J.H. Cockayne, Proc. R. Soc. London, Ser. A **325**, 543 (1971).

[6] F. Häussermann and H. Schaumburg, Philos. Mag. **27**, 745 (1973).

[7] A. Gomez, D.J.H. Cockayne, P.B. Hirsch, and V. Vitek, Philos. Mag. **31**, 105 (1975).

[8] K. Wessel and H. Alexander, Philos. Mag. **35**, 1523 (1977).

[9] P.N. Keating, Phys. Rev. **145**, 637 (1966).

[10] W. Weber, Phys. Rev. B **15**, 4789 (1977).

[11] J. Wilder, Diploma thesis, University of Göttingen, 1995.
[12] G.A. Baraff and M. Schlüter, Phys. Rev. B **19**, 4965 (1979).
[13] J. Bernholc *et al.*, Phys. Rev. B **21**, 3545 (1980).
[14] Wang Yong-L. and U. Lindefelt, Phys. Rev. B **37**, 1320 (1988).
[15] R. Jones and T. King, Philos. Mag. B **47**, 491 (1983).
[16] L.F. Mattheiss and J.R. Patel, Phys. Rev. B **23**, 5384 (1981).
[17] S. Marklund, Phys. Status Solidi B **108**, 97 (1981).
[18] N. Lehto, S. Marklund, and Wang Yong-L., Solid State Commun. **92**, 987 (1994).
[19] M.Y. Chou, M.L. Cohen, and S.G. Louie, Phys. Rev. B **32**, 7979 (1981).
[20] K.W. Lodge *et al.*, Philos. Mag. A **60**, 643 (1989).